THE JOURNAL OF PHYSICAL CHEMISTRY C

ARTICLE

pubs.acs.org/JPCC

Quantum Chemical Prediction of Reaction Pathways and Rate Constants for the Reactions of O_x (x = 1 and 2) with Pristine and Defective Graphite (0001) Surfaces

S. C. Xu,[†,∥] Hui-Lung Chen,[‡] and M. C. Lin*[,†,§]

[†]Cherry L. Emerson Center for Scientific Computation and Department of Chemistry, Emory University, Atlanta, Georgia 30322, United States

[‡]Department of Chemistry and Institute of Applied Chemistry, Chinese Culture University, Taipei, 111, Taiwan

[§]Institute of Molecular Science, Department of Applied Chemistry, National Chiao Tung University, Hsichu, Taiwan 300

Supporting Information

ABSTRACT:

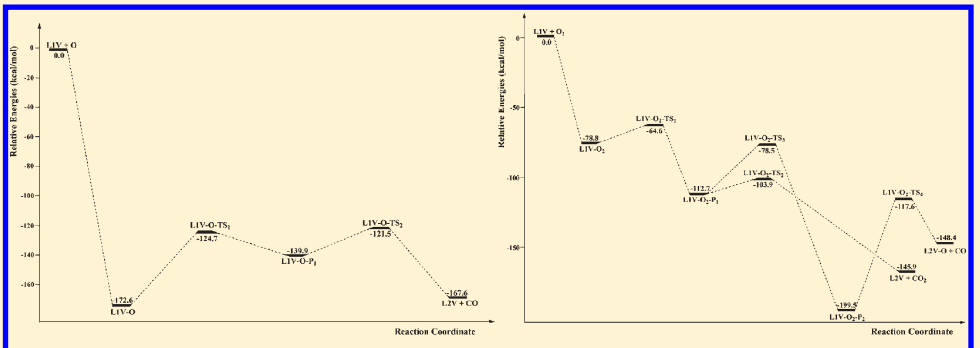

The PESs for the reactions of O and O_2 on the L1V surface

We present reaction pathways for adsorption reactions of the O atom and O_2 molecule in the pristine and monovacancy defective graphite (0001) based on quantum chemical potential energy surfaces (PESs) obtained by the dispersion-augmented density-functional tight-binding (DFTB-D) method. We use a dicircumcoronene $C_{96}H_{24}$ (**L0D**) graphene slab as the pristine graphite (0001) model and dicircumcoronene $C_{95}H_{24}$ (**LIV**) as the graphite (0001) monovacancy defect model. We found that the adsorption reactions of O and O_2 on the **L0D** surface can produce defects on the graphite surface. O can yield CO, while O_2 can yield both CO and CO_2 molecules. The adsorption reactions of the O and O_2 on the **LIV** surface can produce a 2-C defective graphite surface and CO, and CO and CO_2, respectively. The O and O_2 more readily oxidize the defected surface, **LIV**, than the defect-free surface, **L0D**. On the basis of the computed reaction pathways, we predict reaction rate constants in the temperature range between 300 and 3000 K using Rice−Ramsperger−Kassel−Marcus (RRKM) theory. High-temperature quantum chemical molecular dynamics simulations at 3000 K based on on-the-fly DFTB-D energies and gradients support the results of our PES studies.

1. INTRODUCTION

Graphite is an important surface lining material for systems operating under high temperature and high pressure and is being tested as surface material for rocket nozzles[1] and for plasma divertors in nuclear fusion technology.[2]Despite the importance of these technologies, not much is known about the high-temperature, high-pressure (high-T,P) processes causing graphite erosion due to reactions with oxidizing agents from fuel combustion, most importantly H_2O and CO_2.[1]Recently, numerical simulations have given insight into the dynamics of reactive turbulent combustions that stress the importance of O_xH_y (x = 1,2, y = 0−2) species.[3]With most modern fuels, not only O_xH_y but also CO_x and NO_x (x = 1,2) are exhaust species that are the most likely candidates for inducing graphite erosion. In addition, an experimental investigation for the nitrogen adsorption on defects of carbon black surfaces at 77 K by surface spectroscopy (SIMS)[4] was reported and compared with theoretical results obtained by the grand canonical Monte Carlo simulations.[4] It was found that nitrogen adsorption was sensitive to the defects and was enhanced at low temperature and high pressure. Recently, the chemical functionalization of semiconducting graphene nanoribbons (GNRs) with Stone−Wales (SW) defects by carboxyl (COOH) groups has been investigated using density functional theory.[5]It was found that the geometrical structures and electronic properties of the GNRs changed significantly, and the electrical conductivity of the system could

Received: July 20, 2011
Revised: November 8, 2011
Published: December 07, 2011

dx.doi.org/10.1021/jp206934r | J. Phys. Chem. C 2012, 116, 1841−1849

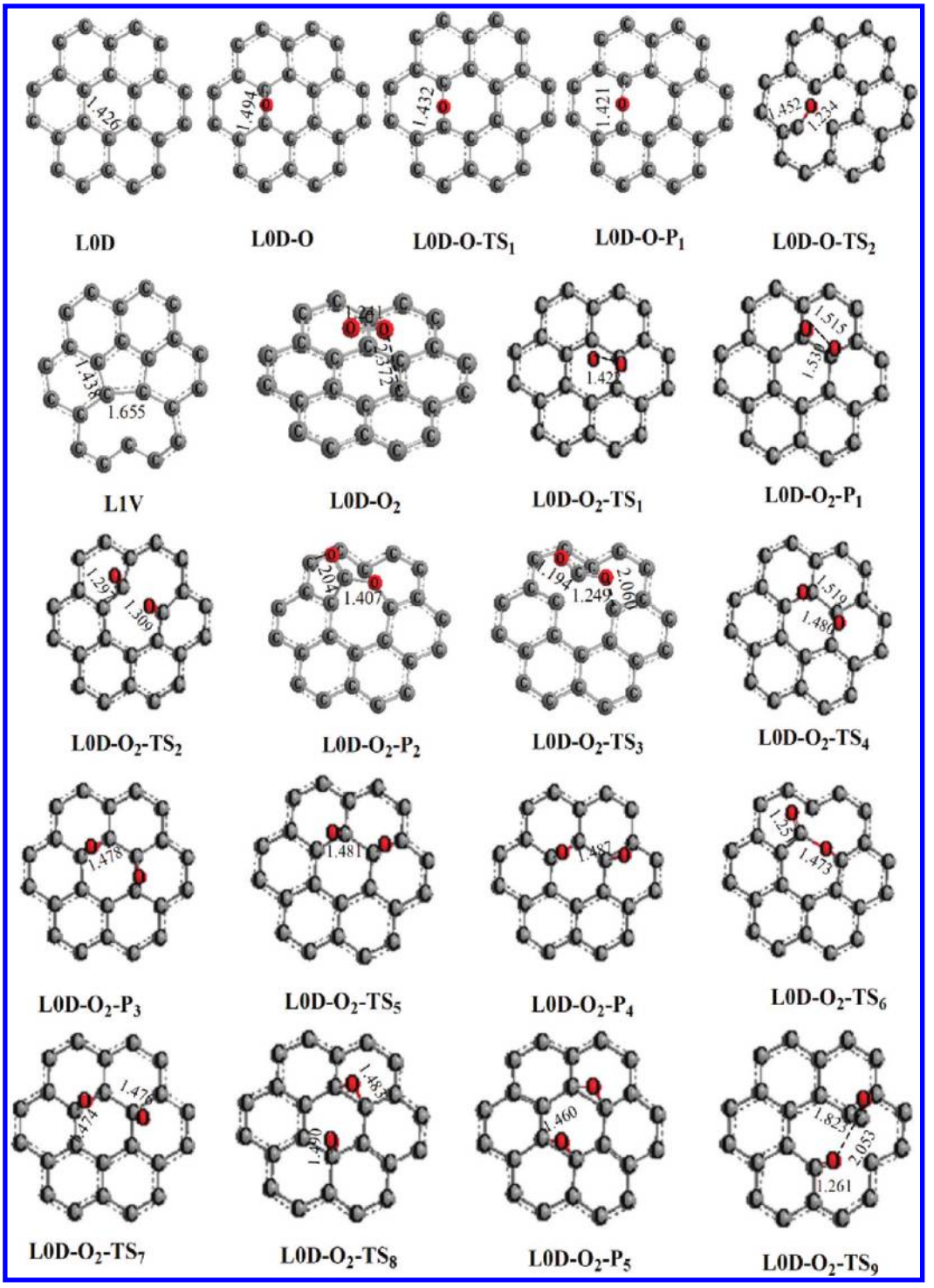

Figure 1. Local structures for the dissociative adsorption of O_x (x = 1 and 2) on the pristine graphite **L0D** model calculated at the DFTB-D level. The unit for the bond lengths is Å.

be considerably enhanced by monoadsorption and double adsorption of COOH, depending sensitively upon the axial concentration of SW defects COOH pairs (SWDCPs). How graphite defect formation occurs under the high-T,P conditions is still not completely understood. Knowledge of these processes is a prerequisite for the improvement of both graphite-based nozzle lining material and the chemical composition of the fuel.

Some time ago, we developed a methodology that allows us to systematically investigate a priori high-T,P dissociative adsorption processes on the basal graphite surface.[6] This methodology uses for the description of the graphite (0001) surface the dicircumcoronene $C_{96}H_{24}$ finite-size graphene flake, optionally stacked up to trilayers, and employs density functional theory (DFT) as well as density functional tight binding[7,8] augmented with London dispersion (DFTB-D)[9,10] quantum chemical

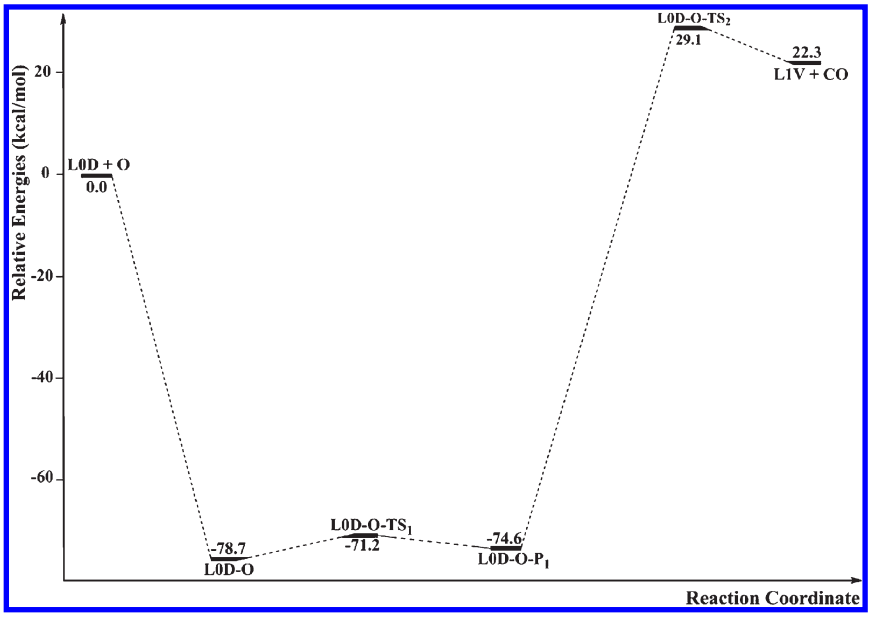

Figure 2. Schematic drawing of the potential energy surfaces for the dissociative adsorption pathways of O on the pristine graphite **L0D** model calculated at the DFTB-D level.

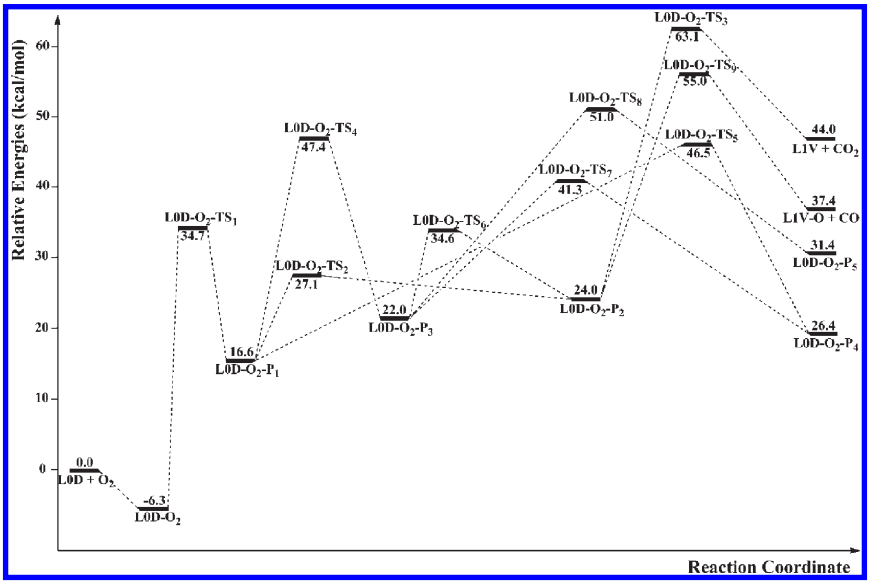

Figure 3. Schematic drawing of the potential energy surfaces for the dissociative adsorption pathways of O_2 on the pristine graphite **L0D** model calculated at the DFTB-D level.

methods for the exploration of the dissociative adsorption potential energy surfaces (PESs). Beginning from stationary points along the reaction pathways, DFTB-D-based molecular dynamics (QM/MD) are then performed at constant temperature to check whether most important reaction pathways have been considered, and finally reaction rate constants are predicted for a wide range of temperatures, based on the Rice−Ramsperger−Kassel−Marcus (RRKM) theory.[11,12] Using this methodology, we predicted high-T,P dissociative adsorption processes and their reaction kinetics for H_2O,[6] CO_x,[13,14] and NO_x[14] (x = 1,2) on the defect-free graphite (0001) surface and those of OH_x,[15] CO_x,[16] and NO_x[17] (x = 1,2) species on the basal face of graphite containing monovacancy defects. In short, we found that on an intact graphene surface H_2O[6] and even more so the radical species NO and NO_2 can cause irreversible oxide defects on the graphite surface,[14] with gaseous CO leaving as a thermodynamically highly stable and highly entropic erosion product. Likewise, the OH radical readily leaves a hydrogenated monovacancy defect (model **L1H1V** in ref 15) behind. We further noticed a pathway for nitridation in the case of NO attack.[14] In the investigation of dissociative adsorptions on various defective models, we found that attacks on the monovacancy defect have generally much lower barriers than corresponding reactions on the defect-free graphite surface.[15−17] In the case of reactions of CO and CO_2 with monovacancy defects, we found that the CO molecule reacts readily with the monovacancy defects and partially "heals" the carbon hexagon network leading to the formation of a stable epoxide, whereas CO_2 oxidizes the defect

dx.doi.org/10.1021/jp206934r |J. Phys. Chem. C 2012, 116, 1841–1849

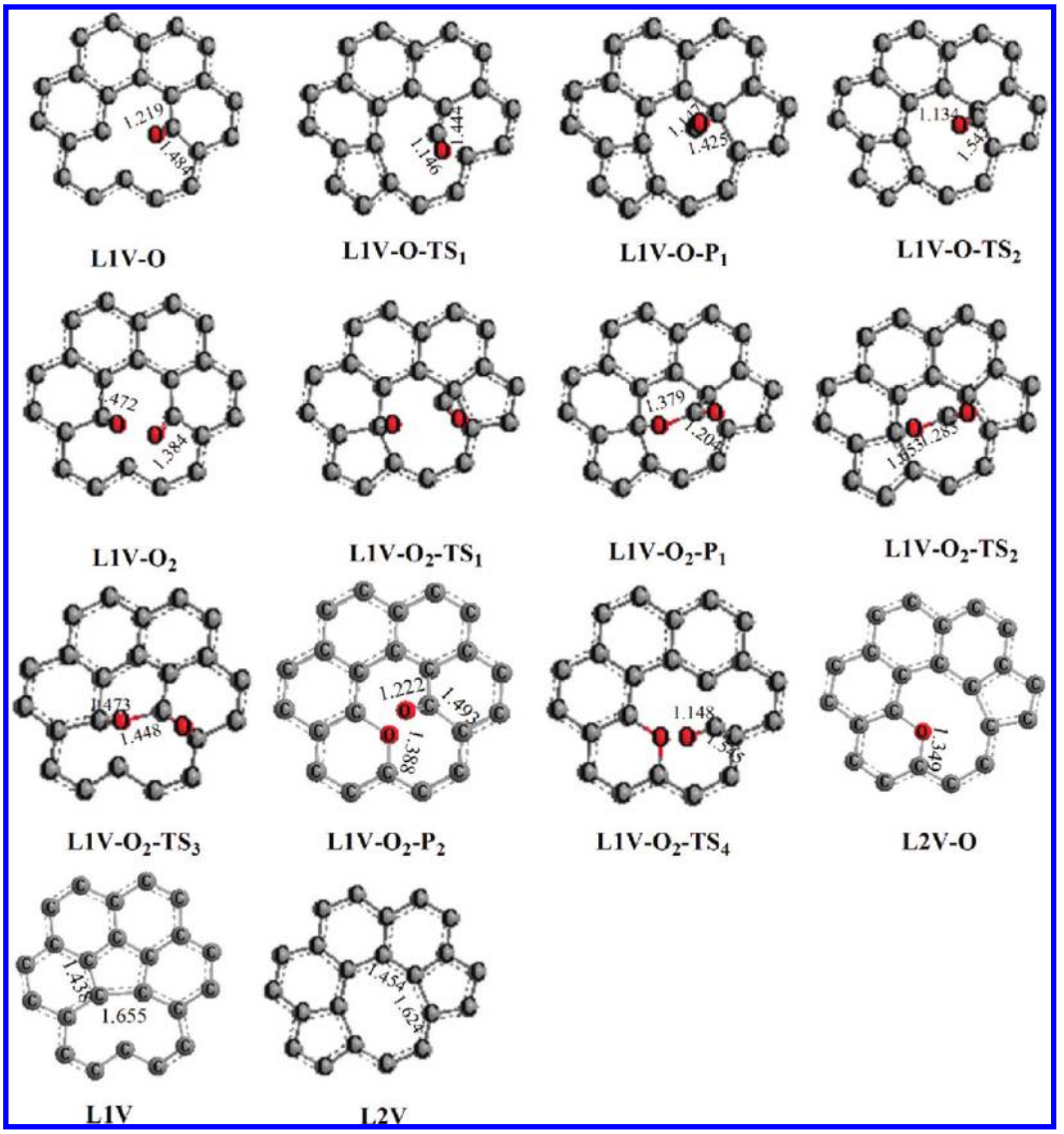

Figure 4. Local structures for the dissociative adsorption of O_x (x = 1 and 2) on the defective graphite **L1V** model calculated at the DFTB-D level. The unit for the bond lengths is Å.

via a dissociative adsorption pathway following CO elimination.[16] In the case of reactions of NO and NO_2 with monovacancy defects, we found that the reactions of NO_x on the monodefective graphite surface were initiated by rapid association processes with negligible barriers, leading to nitridation and oxidation of the graphite surface and eventually producing gaseous CO_x, NO, and CN species leaving from an even more defective graphite surface.[17]

The interactions and reactions for O_x (x = 1 and 2, atomic or molecular oxygen) with graphite have brought great interest to scientists because of important applications of graphite since the 1960s. Experimentally, Gleit et al. reported the reaction kinetics of atomic oxygen with graphitic carbon in the temperature range of 215−300 °C.[18] Blyholder and Eyring reported the kinetics of graphite oxidation using O_2 in the temperature range of 600−1300 °C.[19,20] Bennett et al. have investigated the vacuum ultraviolet photodissociation of molecular oxygen physisorbed on graphite.[21] Theoretically, Incze et al. reported the first-principles studies of the atomic oxygen adsorption on the (0 0 0 1) graphite surface and oxidation of graphite by atomic oxygen.[22,23] Lamoen et al.[24] and Sorescu et al.[25] reported theoretical studies of molecular oxygen adsorption on graphite. Sendt and Haynes reported density functional study of the chemisorption of O_2 on the zigzag surface of graphite.[26] Recently, Paci et al.[27] reported the theoretical direct dynamics based on density functional theory (DFT) and beam-surface scattering experiments for studying the reaction between $O(^3P)$ and highly oriented pyrolytic graphite (HOPC). They found that the incoming O atoms can react with the graphite surface and produce CO by direct collision reaction.

In this work, we focus on the adsorption reactions of O_x (x = 1 and 2) with the single-layer pristine model **L0D** ($C_{96}H_{24}$) and the monovacancy defect model **L1 V** ($C_{95}H_{24}$) using the model systems with the same composition and names as in our previous studies of CO_x and NO_x on the pristine and monovacancy defect graphite surfaces,[14,16,17] which are the parts of a series of studies for the adsorption reactions of gas species on the graphite surface.

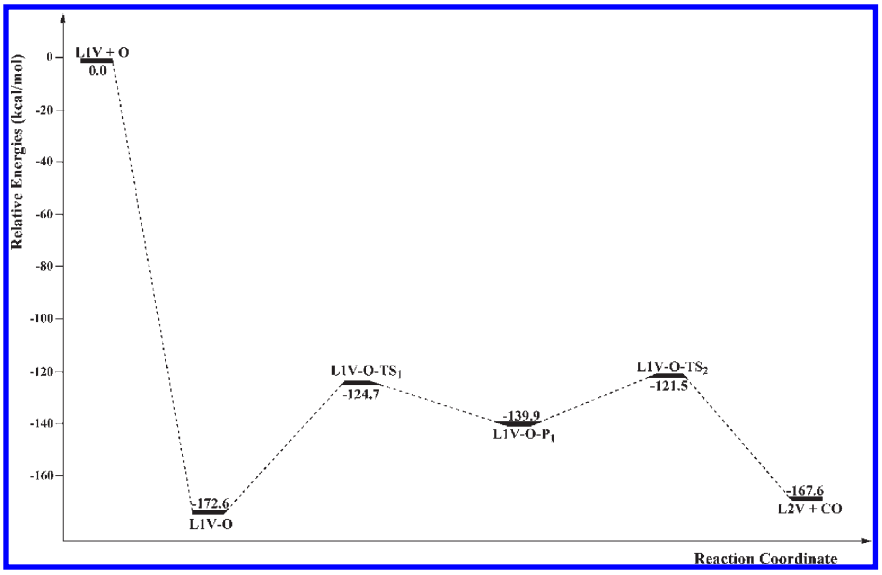

Figure 5. Schematic drawing of the potential energy surfaces for the dissociative adsorption pathways of O on the defective graphite **L1V** model calculated at the DFTB-D level.

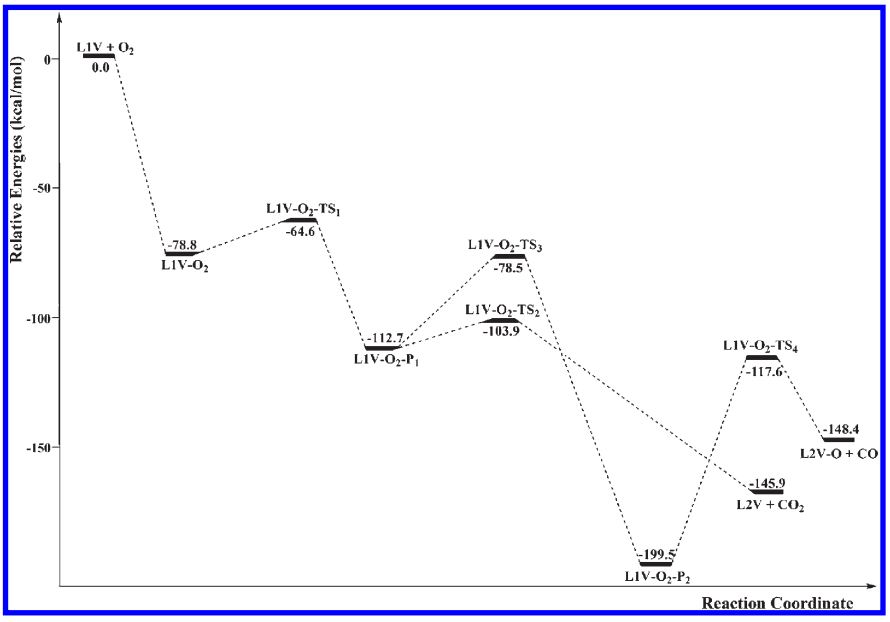

Figure 6. Schematic drawing of the potential energy surfaces for the dissociative adsorption pathways of O_2 on the defective graphite **L1V** model calculated at the DFTB-D level.

2. COMPUTATIONAL METHODOLOGY

In our previous studies of the reactions of CO_x[16] and NO_x[17] (x = 1,2) on the defective model surfaces, we compared the differences in the geometry parameters and energies of the PESs using the B3LYP/6-31+G(d) and DFTB-D methods and those on the different defective graphite **S1V**, **M1V**, and **L1V** models at the DFTB-D level. By comparing the data using the DFTB-D method with those using the B3LYP/6-31+G(d) method computed for CO_x[16] and NO_x[17] (x = 1,2) with the **S1V** model, we found that the average difference between the methods is 6.5 kcal/mol. In this work, the PES exploration of the reaction of O_x on the single-layer pristine model **L0D** ($C_{96}H_{24}$) and monovacancy defect model **L1V** ($C_{95}H_{24}$) was performed using the DFTB-D level of theory. The location of transition states with the DFTB-D method is presently only possible for a finite molecular system. The single-layer **L0D** and **L1V** models are therefore of finite size and are terminated by hydrogen at the edges. For the investigation of small-molecule interactions with graphite surfaces, cluster calculations were employed as well, with members of the coronene family as model systems for individual graphite layers.[28,29] Our previous study[6] found that the DFTB-D method with the finite graphite model was able to reproduce the experimental bulk graphite C−C bond length, interlayer distances, and binding energies of bulk graphite reasonably well.

dx.doi.org/10.1021/jp206934r |J. Phys. Chem. C 2012, 116, 1841–1849

QM/MD simulations at the DFTB-D level were carried out for the dissociation product species of O_x reactions with the **L0D** and **L1V** models, using a Verlet algorithm with a 0.12 fs time step up to 400 steps. This time interval was checked to conserve total energy to within 3 kcal/mol accuracy during microcanonical dynamics with temperature-adjusted initial velocities for 3000 K. In all production trajectories, a target temperature of 3000 K was maintained by using the scaling of velocities approach with 20% overall scaling probability. Although at very high temperatures electronic excitations should be abundant, internal conversion and thereby quenching of electronic excitations due to vibrational excitations is very efficient.[30] We therefore give an approximation that only the electronic ground state in our QM/MD simulations is considered.

For the quantum chemistry calculations, the GAUSSIAN 03 revision C.1[31] was used, and the "external" keyword was employed to perform DFTB-D with a stand alone code. In addition, the reaction rate constants for the adsorption and dissociation reactions have been determined using the ChemRate program.[32]

3. RESULTS AND DISCUSSION

3.1. Adsorption Reaction of O_x on Pristine Graphite. The optimized molecular structures and potential energy surfaces (PESs) for the adsorption reactions of O_x (x = 1 and 2) on the $C_{96}H_{24}$ (**L0D**) surface are presented in Figures 1, 2, and 3, respectively. For the reaction of O + **L0D** shown in Figure 2, the O atom can react directly with the two carbon atoms on the **L0D** surface as a stable adduct L0D-O (an epoxide structure), with a binding energy of 78.7 kcal/mol. Then, the C−C bond in the epoxide ring cleaves to form the **L0D-O-P$_1$** adduct by overcoming a 7.5 kcal/mol barrier at **L0D-O-TS$_1$**. Finally, **L0D-O-P$_1$** can also dissociate to give a gaseous CO and defective graphite **L1V**. This step of the reaction is endothermic by 96.9 kcal/mol and occurs with a 103.7 kcal/mol energy barrier at **L0D-O-TS$_2$**. Therefore, the dissociative adsorption of the O atom on the **L0D** surface can defect the graphite surface and produce CO. For the reaction of O_2 + **L0D** shown in Figure 3, O_2 first absorbs physically on the **L0D** surface as a van der Waals complex **L0D-O$_2$** with a 6.3 kcal/mol binding energy. Then, two O atoms combine with the two closest carbon atoms on the **L0D** surface as a stable adduct **L0D-O$_2$-P$_1$**. This step of the reaction is endothermic by 22.9 kcal/mol and occurs with a 41.0 kcal/mol barrier at **L0D-O$_2$-TS$_1$**. One of O-C-a's in **L0D-O$_2$-P$_1$** migrates and combines with another O-a to form a-O-C-O-a ("a" is defined as carbon atom site) as **L0D-O$_2$-P$_2$**. This process is endothermic by 7.4 kcal/mol and occurs with a 10.5 kcal/mol barrier at **L0D-O$_2$-TS$_2$**. The C−O in **L0D-O$_2$-P$_2$** can dissociate to give off a gaseous CO by overcoming a barrier of 31.0 kcal/mol at **L0D-O$_2$-TS9** and finally form a defective site **LIV-O**. At the same time, the O−C−O in **L0D-O$_2$-P$_2$** can also dissociate to give off a gaseous CO_2 by overcoming a barrier of 39.1 kcal/mol at **L0D-O$_2$-TS$_3$** and finally form a defective site **LIV**. Furthermore, the O-a in **L0D-O$_2$-P$_1$** can shift from one site to a nearby site by isomerization reactions. For example, **L0D-O$_2$-P$_1$** can isomerize to **L0D-O$_2$-P$_3$** with a barrier of 30.8 kcal/mol at **L0D-O$_2$-TS$_4$** or to **L0D-O$_2$-P$_4$** with a barrier of 29.9 kcal/mol at **L0D-O$_2$-TS$_5$**. Further, **L0D-O$_2$-P$_3$** can isomerize to **L0D-O$_2$-P$_2$** with a barrier of 12.6 kcal/mol at **L0D-O$_2$-TS$_6$**, to **L0D-O$_2$-P$_4$** with a barrier of 19.3 kcal/mol at **L0D-O$_2$-TS$_7$**, or to **L0D-O$_2$-P$_5$** with a barrier of 29.0 kcal/mol at **L0D-O$_2$-TS$_8$**. In summary, the dissociative adsorption of O_2 on the **L0D** surface can create a bigger defected ring on the graphite surface and produce a CO_2 molecule.

3.2. Adsorption Reaction of O_x on Defective Graphite. The optimized molecular structures and potential energy surfaces (PESs) for the adsorption reactions of O_x (x = 1 and 2) on the $C_{95}H_{24}$defective model (**L1V**) surface are presented in Figures 4, 5, and 6, respectively. For the O atom on the **L1V** surface shown in Figure 5, it reacts directly with defective graphite **L1V** to form a stable adduct **L1V-O** with a binding energy of 172.6 kcal/mol. Then, **L1V-O** isomerizes to adduct **L1V-O-P$_1$** with an endothermicity of 32.7 kcal/mol. This isomerization occurs by a 47.9 kcal/mol barrier at **L1V-O-TS$_1$**. Finally, **L1V-O-P$_1$** can dissociate to give off a gaseous CO and 2-C defective graphite **L2V** by overcoming a 18.4 kcal/mol barrier at **L1V-O-TS$_2$**. This step of the reaction is exothermic by 27.7 kcal/mol. Therefore, the dissociative adsorption of the O atom on the **LIV** surface can create a 2-C defective graphite surface more easily than that on the **L0D** and produce CO. For the O_2 on the **L1V** surface shown in Figure 6, the O_2 molecule reacts directly with the defective graphite **L1V** to form a stable adduct **L1V-O$_2$** with a binding energy of 78.8 kcal/mol. Then, one of the O-C-a's in **L1V-O$_2$** migrates and combines with the other O-a to form a-O-C-O-a ("a" is defined as a carbon atom site) as **L1V-O$_2$-P$_1$**. This process is exothermic by 33.9 kcal/mol and occurs with a 14.2 kcal/mol barrier at **L1V-O$_2$-TS$_1$**. The O−C−O in **L1V-O$_2$-P$_1$** can dissociate to give off a gaseous CO_2 by overcoming a barrier of 8.8 kcal/mol at **L1V-O$_2$-TS$_2$** and form the 2C-defective graphite **L2V**. This process is exothermic by 33.2 kcal/mol. At the same time, **L1V-O$_2$-P$_1$** can isomerize to **L1V-O$_2$-P$_2$** with a barrier of 34.2 kcal/mol at **L1V-O$_2$-TS$_3$**. This process is exothermic by 86.8 kcal/mol. Finally, The C−O in **L1V-O$_2$-P$_2$** can dissociate to give off a gaseous CO by overcoming a barrier of 81.9 kcal/mol at **L1V-O$_2$-TS$_4$** and form the defective graphite **L2V-O**. This process is endothermic by 51.1 kcal/mol. Therefore, the dissociative adsorption of O_2 on the **L1V** surface can create defective graphite surface **L2V** or **L2V-O** more easily than that on the **L0D** and produce CO_2 and CO.

3.3. Reaction Rate Constants Predicted by the RRKM Theory. The rate constants for these gas−surface reactions have been computed with the RRKM theory using the ChemRate code.[32] The predicted rate constants of the O_x (x = 1 and 2) adsorption reactions on the pristine graphite surfaces are as follows

$$O + L0D \rightarrow L0D\text{-}O \quad (1)$$

$$\rightarrow CO + L1V \quad (2)$$

$$\rightarrow CO + L1V\text{-}O \quad (4)$$

$$\rightarrow CO_2 + L1V \quad (5)$$

The predicted rate constants for the reactions in the temperature range from 300 to 3000 K can be represented by the expressions

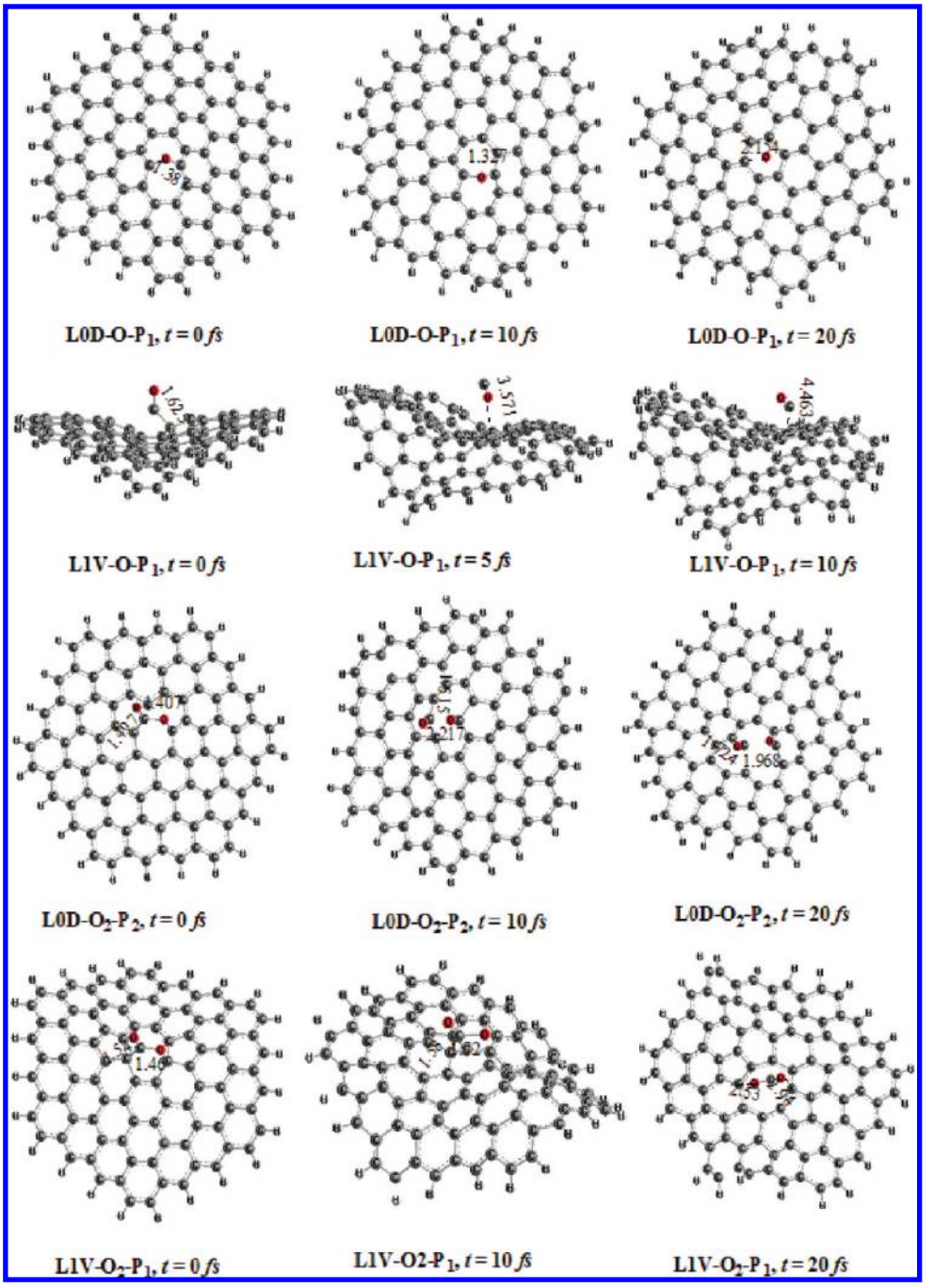

Figure 7. Dynamics structures for the QM/MD simulations of dissociation products of O_x on the **L0D** and **L1V** models at 3000 K using the DFTB-D method. Two trajectories are shown corresponding to different initial geometries. The unit for the bond lengths is Å.

in units of cm^3/s

$$k_1 = 5.29 \times 10^{-7} \times T^{-1.20} \exp(-236/T) \text{ at } T = 300 - 1100 \text{ K},$$
$$k_1 = 1.59 \times 10^{198} \times T^{-58.4} \exp(-78700/T) \text{ at } T = 1100 - 3000 \text{ K},$$
$$k_2 = 7.10 \times 10^{-63} \times T^{15.4} \exp(-16300/T) \text{ at } T = 300 - 1100 \text{ K},$$
$$k_2 = 2.40 \times 10^{240} \times T^{-71.7} \exp(-111500/T) \text{ at } T = 1100 - 3000 \text{ K},$$
$$k_3 = 4.29 \times 10^{-14} \exp(-19700/T),$$
$$k_4 = 3.03 \times 10^{-12} \exp(-30700/T),$$
$$k_5 = 1.27 \times 10^{-11} \exp(-34800/T)$$

The predicted rate constants of the O_x (x = 1 and 2) adsorption reactions on the defective graphite surfaces are as follows

$$O + L1V \rightarrow CO + L2V \quad (6)$$

$$O_2 + L1V \rightarrow L1V\text{-}O_2 \quad (7)$$

$$\rightarrow CO_2 + L2V \quad (8)$$

$$\rightarrow CO + L2V\text{-}O \quad (9)$$

The predicted rate constants for the reactions in the temperature range from 300 to 3000 K can be represented by the expressions

dx.doi.org/10.1021/jp206934r |J. Phys. Chem. C 2012, 116, 1841–1849

in units of cm^3/s

$$k_6 = 4.36 \times 10^{32} \times T^{-15.3} \exp(-9218/T) \text{ at } T = 300 - 1100 \text{ K},$$

$$k_6 = 1.20 \times 10^{221} \times T^{-70.3} \exp(-62900/T) \text{ at } T = 1100 - 3000 \text{ K},$$

$$k_7 = 6.51 \times 10^{-63} \times T^{-0.11} \exp(340/T) \text{ at } T = 300 - 1100 \text{ K},$$

$$k_7 = 7.30 \times 10^{178} \times T^{-53} \exp(-65000/T) \text{ at } T = 1100 - 3000 \text{ K},$$

$$k_8 = 9.13 \times 10^{-83} \times T^{21.9} \exp(-6800/T) \text{ at } T = 300 - 1100 \text{ K},$$

$$k_8 = 2.00 \times 10^{230} \times T^{-68.0} \exp(-100900/T) \text{ at } T = 1100 - 3000 \text{ K},$$

$$k_9 = 3.03 \times 10^{-83} \times T^{21.9} \exp(-18400/T) \text{ at } T = 300 - 1100 \text{ K},$$

$$k_9 = 2.08 \times 10^{229} \times T^{-68.4} \exp(-112400/T) \text{ at } T = 1100 - 3000 \text{ K}$$

The rate constants (k_i) for the adsorption reactions of O_x on graphite are defined by[33]

$$d[X]_{surf}/dt = k_i(\theta/A_s)[X]_g$$

which has the unit of a flux, molecule/(cm^2 s). In the rate equation, θ represents the fraction of available surface sites; A_s is the surface area; and $[X]_g$ is the gas phase concentration of O_x in molecules/cm^3.

In comparison, the rate constant for the adsorption of the O on the monodefective graphite surface for creating CO at 1000 K is 5.75×10^5 times faster than that on the defect-free graphite surface but 9.16×10^6 times slower than that of the NO on the monodefective graphite surface.[17] The rate constant of the O_2 on the monodefective graphite surface for creating CO_2 at 1000 K is 5.21×10^6 times faster than on the defect-free graphite surface but is 3.00×10^{16}times slower than that of the NO_2 on the monodefective graphite surface.[17] Therefore, by predicting rate constants of O_x on the graphite surface, we can learn quantitatively how fast the reactions of O_x on the graphite surface are, providing us a guideline for related experimental investigations.

3.4. QM/MD Simulations of O_x Dissociative Products on the Pristine and Defective Graphite Surfaces. QM/MD constant-temperature simulations of the dissociative products of O_x on the surfaces of the **L0D** and **L1V** models as described above were carried out using the DFTB-D quantum chemical potential at a temperature of 3000 K. When the temperature is higher than 3000 K, the enthalpy and heat capacity of graphite increase slowly,[34] so 3000 K is a standard temperature for simulating the high-temperature property of graphite, In the following, we describe the details of these simulations.

QM/MD simulations starting from the dissociative products of **L0D-O-P$_1$** and **L0D-O$_2$-P$_2$** for O_x on the pristine graphite surface were carried out, and some snapshots of trajectories are shown in Figure 7. As can be seen from Figure 7, for **L0D-O-P$_1$**, the O atom has formed strong bridge bonds with graphitic carbons. After 10 fs, the O−C bridge bonds change a little, and after 20 fs, the O atom moved up on the surface and still sticks with surface carbons. The local graphite recovered to 6−6 pristine rings. In the whole simulation, we did not see CO fragmenting out because the dissociation barrier for producing CO is too high. For **L0D-O$_2$-P$_2$**, the CO bond in OC−O was broken after 10 fs, and after 20 fs CO moved up to the surface giving the gaseous CO product.

The QM/MD simulations for the dissociative products of **L1V-O-P$_1$** and **L1V-O$_2$-P$_1$** for O_x on the defective graphite surface are also shown in Figure 7. For **L1V-O-P$_1$**, CO in **L1V-O-P$_1$** dissociated away from the surface and produced gaseous CO after 5 fs. This result is in good agreement with the previous study by the DFT dynamics simulation,[27] which has shown that the O atoms on the single-atom vacancy graphene surface can produce CO. For **L1V-O$_2$-P$_1$**, CO_2 moved up to the surface after 10 fs, and after 20 fs, CO_2 dissociated away from the surface and produced gaseous CO_2. In summary, our results from the QM/MD simulations of O_x on the pristine and defective graphite as well as graphene surfaces have indicated that reaction paths in the simulations easily followed the minimum energy paths shown in the dissociative adsorption PESs.

4. CONCLUSIONS

The reactions of the O atom and O_2 molecule on the pristine and monovacancy defective graphite surface were calculated using the DFTB-D method. The PESs for the adsorption reactions of O_x (x = 1 and 2) on the pristine and defective graphite were computed, and intermediate structures, transition states, and low-lying product structures were characterized. For the adsorption of O and O_2 on the pristine graphite, we found that O_x can defect the graphite surface. O can yield CO, while O_2 can yield CO and CO_2 molecules. For the adsorption of the O and O_2 on the **LIV** surface, we found that they can produce a 2-C defective graphite surface and CO and CO and CO_2, respectively. The O and O_2 more readily oxidize the defected surface, **LIV**, than the defect-free surface, **L0D**. On the basis of the TS structures, frequencies, and energetics, we also predict the rate constants of the adsorption reactions of O_x on the pristine and defective graphite using RRKM. Quantum chemical molecular dynamics (QM/MD) simulations at the DFTB-D level of theory were also carried out for reaction products to elucidate reverse adsorption pathways and to further explore the PESs accessible at T = 3000 K. The QM/MD simulations of O_x on the pristine and defective graphite surfaces are consistent with the PES results. Overall, we conclude that O_x can oxidize much more easily the monovacancy defective graphite (0001) surface than the defect-free graphite and produce gaseous CO and CO_2 species. Chain reactions of these product species may occur afterward, leading to further erosion of the graphite surface.

■ ASSOCIATED CONTENT

Supporting Information. Table S1 lists names, the DFTB-D total energies, and imaginary frequencies for all structures of the reaction pathways, and Table S2 lists corresponding Cartesian coordinates. Figure S1 shows the models **S1V**, **M1V**, and **L1V**. This material is available free of charge via the Internet at http://pubs.acs.org.

■ AUTHOR INFORMATION

Corresponding Author

*E-mail: chemmcl@emory.edu.

Present Addresses

‖School of Chemistry and Biochemistry, Georgia Institute of Technology. E-mail: sxu65@mail.gatech.edu.

■ ACKNOWLEDGMENT

We gratefully acknowledge financial support from the Office of Naval Research under a MURI grant. MCL acknowledges

support from the Taiwan Semiconductor Manufacturing Co. (TSMC) and the National Science Council of Taiwan for a Distinguished Visiting Professorship at the National Chiao Tung University in Hsinchu, Taiwan. We thank the Cherry L. Emerson Center for Scientific Computation at Emory University for valuable computer time.

REFERENCES

(1) Keswani, S. T.; Andiroglu, E.; Campbell, J. D.; Kuo, K. K. *J. Spacecr. Rockets* **1985**, *22*, 396.
(2) Federici, G.; Skinner, C. H.; Brooks, J. N.; Coad, J. P.; Grisolia, C.; Haasz, A. A.; Hassanein, A.; Philipps, V.; Pitcher, C. S.; Roth, J.; Wampler, W. R.; Whyte, D. G. *Nucl. Fusion* **2001**, *41*, 1967.
(3) Hawkes, E. R.; Sankaran, R.; Sutherland, J. C.; Chen, J. H. *J. Phys. Conf. Ser.* **2006**, *16*, 65.
(4) Darmstadt, H.; Roy, C. *Carbon* **2001**, *39*, 841.
(5) OuYang, F.; Huang, B.; Li, Z.; Xu, H. *Los Alamos National Laboratory, Preprint Archive, Condensed Matter* **2007**, 1.
(6) Xu, S.; Irle, S.; Musaev, D. G.; Lin, M. C. *J. Phys. Chem. A* **2005**, *109*, 9563.
(7) Porezag, D.; Frauenheim, T.; Koehler, T.; Seifert, G.; Kaschner, R. *Phys. Rev. B* **1995**, *51*, 12947.
(8) Elstner, M.; Porezag, D.; Jungnickel, G.; Elsner, J.; Haugk, M.; Frauenheim, T.; Suhai, S.; Seifert, G. *Phys. Rev. B* **1998**, *58*, 7260.
(9) Elstner, M.; Hobza, P.; Frauenheim, T.; Suhai, S.; Kaxiras, E. *J. Chem. Phys.* **2001**, *114*, 5149.
(10) Kumar, A.; Elstner, M.; Suhai, S. *Int. J. Quantum Chem.* **2003**, *95*, 44.
(11) Kassel, L. S. *J. Phys. Chem.* **1928**, *32*, 225.
(12) Marcus, R. A. *J. Chem. Phys.* **1952**, *20*, 359.
(13) Xu, S.; Irle, S.; Musaev, D. G.; Lin, M. C. *The JANNAF 15th Nondestructive Evaluation/24th Rocket Nozzle Technology/37th Structures and Mechanical Behavior Joint Subcommittee Meeting*, Oct. 31−Nov. 4, 2005.
(14) Xu, S. C.; Irle, S.; Musaev, D. G.; Lin, M. C. *J. Phys. Chem. B* **2006**, *110*, 21135.
(15) Xu, S. C.; Irle, S.; Musaev, D. G.; Lin, M. C. *J. Phys. Chem. C* **2007**, *111*, 1355.
(16) Xu, S. C.; Irle, S.; Musaev, D. G.; Lin, M. C. *J. Phys. Chem. C* **2009**, *113*, 18772.
(17) Xu, S. C.; Irle, S.; Lin, M. C. *J. Phys. Chem. C* **2010**, *114*, 8375.
(18) Gleit, C. E.; Holland, W. D.; Wrigley, R. C. *Nature* **1963**, *200*, 69.
(19) Blyholder, G. D.; Eyring, H. *J. Phys. Chem.* **1959**, *63*, 1004.
(20) Blyholder, G. D.; Eyring, H. *J. Phys. Chem.* **1957**, *61*, 682.
(21) Bennett, R. A.; Bennett, S. L.; Siller, L.; MacDonald, M. A.; Palmer, R. E.; Wright, H. M.; Foord, J. S. *J. Phys.: Condens. Matter* **1994**, *6*, 1955.
(22) Incze, A.; Pasturel, A.; Chatillon, C. *Surf. Sci.* **2003**, *537*, 55–63.
(23) Incze, A.; Pasturel, A.; Chatillon, C. *Appl. Surf. Sci.* **2001**, *177*, 226.
(24) Lamoen, D.; Persson, B. N. J. *J. Chem. Phys.* **1998**, *108*, 3332.
(25) Sorescu, D. C.; Jordan, K. D.; Avouris, P. *J. Phys. Chem. B* **2001**, *105*, 11227.
(26) Sendt, K.; Haynes, B. S. *Combust. Flame* **2005**, *143*, 629.
(27) Paci, J. T.; Upadhyaya, H. P.; Zhang, J.; Schatz, G.; Minton, T. *J. Phys. Chem. A* **2009**, *113*, 4677.
(28) Feller, D.; Jordan, K. D. *J. Phys. Chem. A* **2000**, *104*, 9971.
(29) Bauschlicher, C. W., Jr.; Ricca, A. *Phys. Rev. B* **2004**, *70*, 115409/1.
(30) Schwen, D.; Bringa, E. M. *Nucl. Instrum. Methods Phys. Res., Sect. B* **2007**, *256*, 187.
(31) Frisch, M. J.; Trucks, G. W.; Schlegel, H. B.; Scuseria, G. E.; Robb, M. A.; Cheeseman, J. R.; Montgomery, J. A., Jr.; Vreven, T.; Kudin, K. N.; Burant, J. C.; Iyengar, S. S.; Millam, J. M.; Tomasi, J.; Barone, V.; Mennucci, B.; Cossi, M.; Scalmani, G.; Rega, N.; Petersson, G. A.; Ehara, M.; Toyota, K.; Hada, M.; Fukuda, R.; Hasegawa, J.; Ishida, M.; Nakajima, T.; Kitao, O.; Nakai, H.; Honda, Y.; Nakatsuji, H.; Li, X.; Knox, J. E.; Hratchian, H. P.; Cross, J. B.; Adamo, C.; Jaramillo, J. J.; Cammi, R.; Pomelli, C.; Gomperts, R.; Stratmann, R. E.; Ochterski, J.; Ayala, P. Y.; Morokuma, K.; Salvador, P.; Dannenberg, J. J.; Zakrzewski, V. G.; Dapprich, S.; Daniels, A. D.; Strain, M. C.; Farkas, O.; Malick, D. K.; Rabuck, A. D.; Raghavachari, K.; Foresman, J. B.; Ortiz, J. V.; Cui, Q.; Baboul, A. G.; Clifford, S.; Cioslowski, J.; Stefanov, B. B.; Liu, G.; Liashenko, A.; Piskorz, P.; Komaromi, I.; Martin, R. L.; Fox, D. J.; Keith, T.; Al-Laham, M. A.; Peng, C. Y.; Nanayakkara, A.; Challacombe, M.; Gill, P. M. W.; Johnson, B.; Chen, W.; Wong, M. W.; Gonzalez, C.; Pople, J. A. *Gaussian 03*, Revision C.1ed.; Gaussian, Inc.: Pittsburgh, PA, 2004.
(32) Mokrushin, W.; Bedanov, V.; Tsang, W.; Zachariah, M.; Knyazev, V. *ChemRate*, Version 1.20; National Institute of Standards and Technology: Gaithersburg, MD 20899, U.S.A, 2003.
(33) Rettner, C. T.; Ashfold, M. N. R. *Dynamics of Gas-Surface Interactions* (Chapter 5, Kinetics of Surface Reactions); The Royal Society of Chemistry: U.K., 1991.
(34) Butland, A. T. D.; Maddison, R. J. *J. Nucl. Mater.* **1974**, *49*, 45.